Ab Initio Studies of ClO_x Reactions. 2. Unimolecular Decomposition of s-ClO_3 and the Bimolecular O + OClO Reaction†

R. S. Zhu and M. C. Lin*

Emory University, Atlanta, Georgia 30322

Received: January 9, 2002; In Final Form: March 15, 2002

The unimolecular decomposition of symmetric ClO_3 has been investigated at the G2M(CC2)//PW91PW91/6-311+G(3df) level of theory. The results show that the main dissociation products are ^3O + OClO instead of the commonly assumed ClO + O_2. The rate constants at high- and low-pressure limits were predicted to be $k_2^\infty = 1.5 \times 10^{20}T^{-1.1}$ exp(−18360/*T*) s^{-1} and $k_2^0 = 3.76 \times 10^{25}T^{-3.28}$ exp(−13890/*T*) cm^3 mol^{-1} s^{-1} in the temperature range 500−2500 K. For the bimolecular processes, the sum of the predicted abstraction (k_3) and association (k_{-2}) values can reasonably explain the experimental nonzero intercepts of the strong pressure-dependent rate constants, with the predicted total rate constants agreeing closely with the experimental values. The association and abstraction rate constants in the temperature range 200−500 K can be represented respectively by $k_{-2} = 40.1T^{-6.16}$ exp(−403/*T*) for 1 Torr He and $k_3 = 1.0 \times 10^{-16}T^{1.44}$ exp(−469/*T*) cm^3 $molecule^{-1}$ s^{-1}. The abstraction rate constant for 500−2500 K can be expressed by $k_3 = 8.69 \times 10^{-17}T^{1.45}$ exp(−441/*T*) cm^3 $molecule^{-1}$ s^{-1}.

I. Introduction

Chlorine dioxide (OClO) and chlorate radical (s-ClO_3) are key reactive intermediates involved in the initiation process of ammonium perchlorate (AP) propellant combustion reaction.[1] These species, particularly the former, may also participate in the ozone depletion chemistry by Freons in the stratosphere.[2] In the combustion of AP, the chlorate radical can be formed directly by the unimolecular decomposition of perchloric acid ($HClO_4$),[3] whereas in the stratosphere, it may be formed by the O + OClO and XO + OClO (X = Cl, Br, and O_2) reactions, for example. The decomposition of the s-ClO_3 radical has been assumed to occur primarily by the O_2 molecular elimination path:[4]

$$\text{s-}ClO_3 \rightarrow ClO + O_2 \qquad (1)$$

whose rate constant has not been determined experimentally. In principle, the decomposition reaction can also take place by the production of an O atom, accompanied by OClO; viz.,

$$\text{s-}ClO_3 \rightarrow O + OClO \qquad (2)$$

The reaction is accessible energetically on the basis of the known thermochemistry and the expected large entropy of activation (vide infra).

Experimentally, the O + OClO reaction has been investigated by a number of research groups.[5−10] Colussi[6] first analyzed his kinetic data in terms of the direct abstraction and the combination reaction (−2):

$$O + OClO \rightarrow ClO + O_2 \qquad (3)$$

$$O + OClO \rightarrow \text{s-}ClO_3\,(+M) \qquad (-2)$$

treating (−2) as a third-order process. Reaction 3 was later revised and assumed to be an indirect metathetical process occurring exclusively by the decomposition of the chemically activated s-ClO_3 via the transition state of reaction 1 by Colussi, Sander, and Friedl.[7] In a detailed study by Stief and co-workers in the temperature range 200−400 K at 1−5 Torr He pressure,[8] the occurrence of reaction 3 was confirmed, however. Their low-pressure data exhibit a V-shaped Arrhenius plot, suggesting the convolution of contributions from the direct and combination reactions represented by (3) and (−2), respectively. More recently, Ravishankara and co-workers detected a broad UV absorption peaking at 260 nm, which was attributed to a product formed in the photolysis of OClO, presumably from the O + OClO reaction.[9]

In this study, we examine the mechanism for the unimolecular decomposition of s-ClO_3 and the bimolecular O + OClO reaction quantum chemically using the PW91PW91/6-311+G-(3df) method for geometry optimization and the G2M(CC2) method[11] for energy calculations. The results of this study clearly support the concurrent occurrence of both types of reactions, the direct abstraction, and indirect association/stabilization processes, as concluded by Stief and co-workers.[8] Our results also rule out the importance of reaction 1 in both thermally and chemically activated systems because of its high O_2-elimination barrier. The results of this first comprehensive theoretical study are presented herein.

II. Computational Methods

Ab Initio Calculations. The geometry of the reactants, intermediates, transition states, and products of the ^3O + OClO reaction was computed at the PW91PW91/6-311+G(3df) with Perdew-Wang[12] functionals for exchange and correlation (PW91PW91). Vibrational frequencies employed to characterize stationary points, zero-point energy (ZPE) corrections have also been calculated at this level of theory, and have been used for the rate constant calculations. Intrinsic reaction coordinate (IRC) calculations[13] have been performed to confirm the connection of each transition state with designated reactants and products.

† Part of the special issue "Donald Setser Festschrift".

* Corresponding author. E-mail address: chemmcl@emory.edu.

10.1021/jp020015e CCC: $22.00 © 2002 American Chemical Society
Published on Web 04/27/2002

The energies of all species were calculated by the G2M method,[11] which uses a series of calculations with PW91PW91/6-311+G(3df) optimized geometries to approximate the CCSD-(T)/6-311+G(3df) level of theory, including a "higher level correction (HLC)" based on the number of paired and unpaired electrons. The total G2M energy with zero-point energy (ZPE) correction is calculated as follows:

$$E[\mathrm{G2M(CC2)}] = E_{\mathrm{bas}} + \Delta E(+) + \Delta E(\mathrm{2df}) + \Delta E(\mathrm{CC}) + \Delta' + \Delta E(\mathrm{HLC,CC2}) + \mathrm{ZPE\ [PW91PW91/6\text{-}311+G(3df)]}$$

$$E_{\mathrm{bas}} = \mathrm{E[PMP4/6\text{-}311G(d,p)]}$$

$$\Delta E(+) = E[\mathrm{PMP4/6\text{-}311+G(d,p)}] - E_{\mathrm{bas}}$$

$$\Delta E(\mathrm{2df}) = E[\mathrm{PMP4/6\text{-}311G(2df,p)}] - E_{\mathrm{bas}}$$

$$\Delta E(\mathrm{CC}) = E[\mathrm{CCSD(T)/6\text{-}311G(d,p)}] - E_{\mathrm{bas}}$$

$$\Delta' = E[\mathrm{UMP2/6\text{-}311+G(3df,2p)}] - E[\mathrm{UMP2/6\text{-}311+G(2df,p)}] - E[\mathrm{UMP2/6\text{-}311+G(d,p)}] - \mathrm{E[UMP2/6\text{-}311G(d,p)]}$$

$$\Delta E(\mathrm{HLC,CC2}) = -5.78n_{\beta} - 0.19n_{\alpha}\ \text{in units of mhartree}$$

where n_α and n_β are the numbers of valence electrons, $n_\alpha \geq n_\beta$. All calculations were carried out with Gaussian 98.[14]

Rate Constant Calculations. The rate constants were computed with a microcanonical variational RRKM (Variflex[15]). The PES calculated at the G2M (CC2)//PW91PW91/6-311+G(3df) level, to be discussed in the next section, was used in the calculation. The component rates were evaluated at the *E*,*J*-resolved level. The effect of pressure was studied by 1-D master equation calculations using the Boltzmann probability of the complex for the J distribution. The master equation was solved by inversion and eigenvalue-solver based approaches for association and dissociation processes, respectively.[16,17] To achieve convergence in the integration over the energy range, an energy grain size of 20 cm^{-1} was used for 200−500 K and 100 cm^{-1} was used for 800−2500 K, these grain sizes provide numerically converged results for all temperatures studies with the energy spanning range from 11 993 cm^{-1} below to 67 500 cm^{-1} above the threshold. The total angular momentum *J* covered the range from 1 to 241 in steps of 10 for the *E*,*J*-resolved calculation. For the barrierless transition states, the Morse potential,

$$E(R) = D_{\mathrm{e}}[1 - \mathrm{e}^{-\beta(R-R_{\mathrm{e}})}]^2$$

was used to represent the potential energy along the minimum energy path of each individual reaction coordinate. In the above equation, *R* is the reaction coordinate (i.e., the distance between the two bonding atoms; O−Cl in this work), D_e is the bond energy excluding zero-point energy, and R_e is the equilibrium value of *R*. For the tight transition states, the numbers of states were evaluated according to the rigid-rotor harmonic-oscillator approximation.

III. Results and Discussion

A. Potential Energy Surface and Reaction Mechanism. The optimized geometries of the reactants, intermediates, transition states, and products are shown in Figure 1, the potential energy diagram obtained at the G2M//PW91PW91/6-311+G(3df) level (zero-point energy included) is presented in Figure 2, the relative energies to ^3O + OClO are compiled in Table 1, and the vibrational frequencies and rotational constants

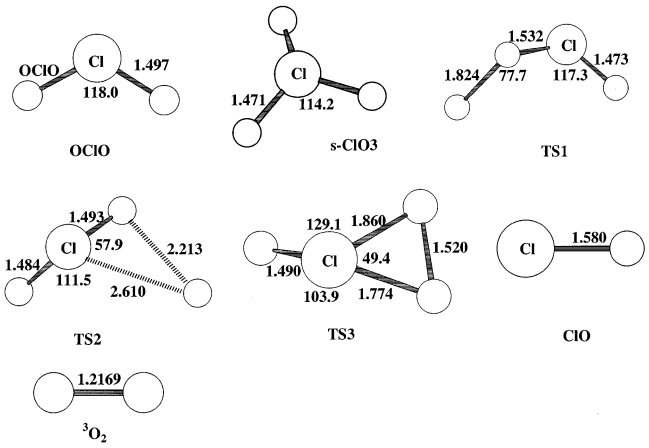

Figure 1. Optimized geometry of the reactants, intermediates, transition states, and products computed at the PW91PW91/6-311+G(3df) level.

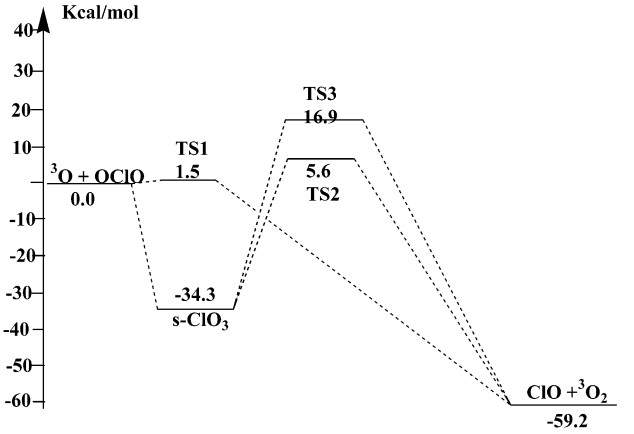

Figure 2. Schematic energy diagram of the s-ClO_3 system computed at the G2M(CC2)//PW91PW91/6-311+G(3df) level.

TABLE 1: Relative Energies Calculated at Various Levels of Theory for ^3O + OClO Reaction Based on the PW91PW91/6-311+G (3df) Optimized Geometry

		ΔE kcal/mol		
species	ZPE, kcal/mol	Pw91pw91/6-311+G(3df)	⟨S^2⟩	G2M//PW91PW91/6-311+G(3df)
^3O + OClO	3.5	0.0		0.0
s-ClO_3	6.3	−49.3	0.75 (0.75)[b]	−34.3 (−34.7)[a]
TS1	4.2	−3.9	0.77 (1.33)[b]	1.5 (3.9)[a]
TS2	4.2	−3.9	1.46 (1.52)[c]	5.6
TS3	4.2	−2.2	0.75 (0.77)[b]	16.9 (16.6)[a]
ClO + $^3O_2$	12.5	−33.3		−59.2 (−59.2)[a]

[a] Numbers in parentheses are based on the G2M//B3LYP/6-311+G(3df) level. [b] Values in parentheses are calculated at the B3LYP/6-311+G(3df) level. [c] This value was obtained at the G96LYP/6-311+G(3df)level; TS2 was not found at the B3LYP/6-311+G(3df) level.

are summarized in Table 2. All energies of this work cited in the text are based on the G2M level.

s-ClO₃. s-ClO_3 has C_{3v} symmetry, and its ground state ($^2A_1$) structure parameters and frequencies have been theoretically studied by various methods.[3,18−23] The Cl−O bond length of s-ClO_3 presents a strong dependence on the methods employed. At the PW91PW91/6-311+G(3df) level employed in this work, the optimized Cl−O bond length is 1.471 Å, which can be compared with 1.454 Å,[3,20,22] 1.510 Å,[19] 1.458 Å,[20] 1.452 Å,[21] 1.449 Å,[23] 1.461 Å,[23] and 1.500 Å,[23] obtained at the B3LYP/6-311+G(3df), QCISD(T)/6-31G(d), CCSD(T)/6-311G(2dp), RB3LYP/cc-pV5Z, MP2/6-311+(2df), SVWN/6-311+G(2df), and G96LYP/6-311+G(2df) levels, respectively. The OClO

TABLE 2: Vibrational Frequencies and Rotational Constants Calculated at the PW91PW91/6−311+G(3df) Level, Which Are Used for Rate Constant Calculations

species	*B*, GHZ	frequencies, cm^{-1}
OClO	50.8, 9.6, 8.1	423, 924, 1071
s-ClO_3 (C_{3v})	9.8, 9.8, 5.2	442 (475), 442 (475), 538 (566), 880 (905) 1043 (1081), 1043 (1081)[a]
TS1	14.4, 5.4, 4.7	693***i***, 211, 314, 425, 861, 1102
TS2	12.8, 4.3, 3.7	227***i***, 109, 170, 434, 910, 1091
TS3	16.9, 5.5, 4.7	540***i***, 216, 326, 502, 872, 1032

[a] Frequencies in parentheses are experimental values from ref 24.

bond angle shows only minor method dependence, which is 114.1 ± 0.1° based on the above methods, except for the value 114.6°,[23] obtained at the MP2/6-311+(2df) level. The PW91PW91/6-311+G(3df) method was used in this work partially because it can provide correct $\langle S^2 \rangle$ for those transition states which are shown in Table 1. From Table 2 one can see that the predicted frequencies at the PW91PW91/6-311+G(3df) level are close to the IR spectral values;[24] the predicted frequencies are only underestimated by 2−7% compared with the experimental ones.[24] The dissociation energy for $ClO_3 \rightarrow {}^3O + OClO$ is predicted to be 34.3 and 34.7 kcal/mol (see Table 1) at the G2M//PW91PW91/6-311+G(3df) and the G2M//B3LYP/6-311+G(3df) levels, respectively, which agree well with the reported value, 34.8 kcal/mol.[19,25]

TS1, TS2, TS3, and Products. Although the s-ClO_3 system has been theoretically studied by several investigators,[3,18−23] its reaction mechanism presented in this section, has not been reported; according to our calculation, there are three channels producing $ClO + {}^3O_2$ from O + OClO. One is a direct bimolecular reaction, in which the O atom attacks one of the O atoms in OClO via TS1 to produce ClO and $^3O_2$ directly. The forming O−O bond length in TS1 is 1.824 Å, the breaking Cl−O bond length increases by 0.035 Å comparing with that in OClO, and the dihedral angle of OClOO is predicted to be 99.8°. For the optimized structure of TS1, the spin contamination is minor at the PW91PW91/6-311+G(3df) level, $\langle S^2 \rangle = 0.77$, comparing with that obtained at the B3LYP/6-311+G(3df) level, $\langle S^2 \rangle = 1.33$ (see Table 1). TS1 lies above the reactants, ^3O + OClO, at 1.5 kcal/mol by G2M//PW91PW91/6-311+G(3df); however, it was predicted to be 1.8 kcal/mol higher at the G2M//B3LYP/6-311+G(3df) level because of the spin contamination problem.

The second and third channels occur by the barrierless O-atom association with OClO to form stable intermediate s-ClO_3, followed by two different dissociation paths: first, one of the Cl−O bond in s-ClO_3 lengthens to 2.610 Å via TS2 (see Figure 1) and abstracts another O atom to give the $ClO + O_2$ products. TS2 has a looser structure, and the spin contamination in TS2 is more serious than that in TS1, $\langle S^2 \rangle$ is 1.46 at the PW91PW91/6-311+G(3df) level. This transition state was not located at the B3LYP/6-311+G(3df) level; however, it was located at the G96LYP/6-311+G(3df) level, but it has higher $\langle S^2 \rangle$, 1.52. The predicted energy lies 5.6 kcal/mol above the reactants at the G2M//PW91PW91/6-311+G(3df). Second, s-ClO_3 dissociates to form $ClO + {}^3O_2$ via a tight transition state TS3 in which two of the Cl−O bonds break concurrently. The breaking bonds lengthen by 0.389 and 0.303 Å compared with those in s-ClO_3. TS3 lies 16.9 and 16.6 kcal/mol above the reactants predicted at the G2M//PW91PW91/6-311+G(3df) and G2M//B3LYP/6-311+G(3df) levels, respectively. This transition state has a higher barrier because of the involvement of two breaking bonds. Therefore, this dissociation channel is kinetically unimportant. The production of $ClO + {}^3O_2$ is exothemic by 59.2 kcal/mol at both the G2M//PW91PW91/6-311+G(3df) and G2M//B3LYP/6-311+G(3df) levels.

Heats of Formation of s-ClO_3 and OClO. To further establish the reliability of the calculations, besides the comparison of frequencies of s-ClO_3 with experimental data in the previous section, here we also compare the predicted heats of formation of s-ClO_3 and OClO with the available calculated or experimental values. The heats of formation at 0 K for ClO, O_2, and ^3O are taken from ref 26 to be 24.15 ± 0.02, 0.0, and 59.0 ± 0.02 kcal/mol, respectively. On the basis of these values and the calculated $\Delta_r H_0$, the heats of formation of s-ClO_3 and OClO are predicted to be 48.6 ± 0.02 and 24.7± 0.04 kcal/mol, respectively. The former value for s-ClO_3 is consistent with the values of 48 kcal/mol obtained at the G1 level by Rathmann and Schindler,[18] 46.0 ± 3.0 kcal/mol obtained at the CCSD(T)/6-311+G(3df)//CCSD(T)/6-311G(2df) level by Workman and Francisco,[20] and 47.2 ± 2.7 kcal/mol based on the reaction of $OH + ClO_3 = HO_2 + OClO$ obtained by Zhu and Lin.[3] The value for OClO, 24.7 kcal/mol, is close to 23.9 ± 1.9 kcal/mol reported in JANAF.[26]

B. Rate Constant Calculations. Variational TST and RRKM calculations have been carried out for this reaction system with the Variflex code[15] including the forward and reverse reactions:

$$\text{s-}ClO_3 \rightarrow ClO + {}^3O_2 \qquad (1)$$

$${}^3O + OClO \leftrightarrow \text{s-}ClO_3{}^* \rightarrow ClO + O_2 \qquad (1')$$

$$\rightarrow \text{s-}ClO_3\ (+M) \qquad (-2)$$

$${}^3O + OClO \rightarrow ClO + O_2 \qquad (3)$$

where * denotes the chemically activated s-ClO_3. The energies used in the calculation are plotted in Figure 2, and the vibrational frequencies and rotational constants are listed in Table 2.

The decomposition of s-ClO_3 forming ^3O and OClO occurs without a well-defined transition state due to the absence of an intrinsic reaction barrier. To predict the dissociation rate reliably, the flexible variational transition state approach originally developed by Marcus and co-workers[27,28] has been employed by means of the Variflex code[15] as alluded to above. The dissociation potential energy for the separation of an O atom from ClO_3 was calculated by varying the Cl−O bond distance from its equilibrium value, 1.484−4.0 Å, with an interval of 0.1 Å. Other geometric parameters were fully optimized without symmetry constrained at the PW91PW91/6-311G(d,p) level of theory. For each structure, we calculated the $3N - 7$ vibrational frequencies, projected out of the gradient direction. The results show that spin contamination occurs at the Cl−O separation near 2.1 Å. The $\langle S^2 \rangle$ value lies between 0.8614 and 1.7140 at the Cl−O distance from 2.1 to 4.0 Å. Several investigators' results[3,29,30] indicated that although spin contamination occurs for a specific bond dissociation of some molecular bonds at the long distance, a smooth and reasonable potential energy surface could be obtained and reasonable rate constants also could be predicted.[3] In this work, the calculated total energy at each point was fitted to a Morse potential energy function given previously and then scaled to match the dissociation energy predicted at the G2M level of theory. The value of β in the Morse potential was determined to be 2.193 $Å^{-1}$ for the dissociation of s-ClO_3. This value will be used in the following rate constant calculation to confirm the reliability of treating this barrierless process.

The Lennard-Jones (L-J) parameters required for the RRKM calculations for s-ClO_3, $\epsilon_1 = 281$ K, and $\sigma_1 = 3.7$ Å were

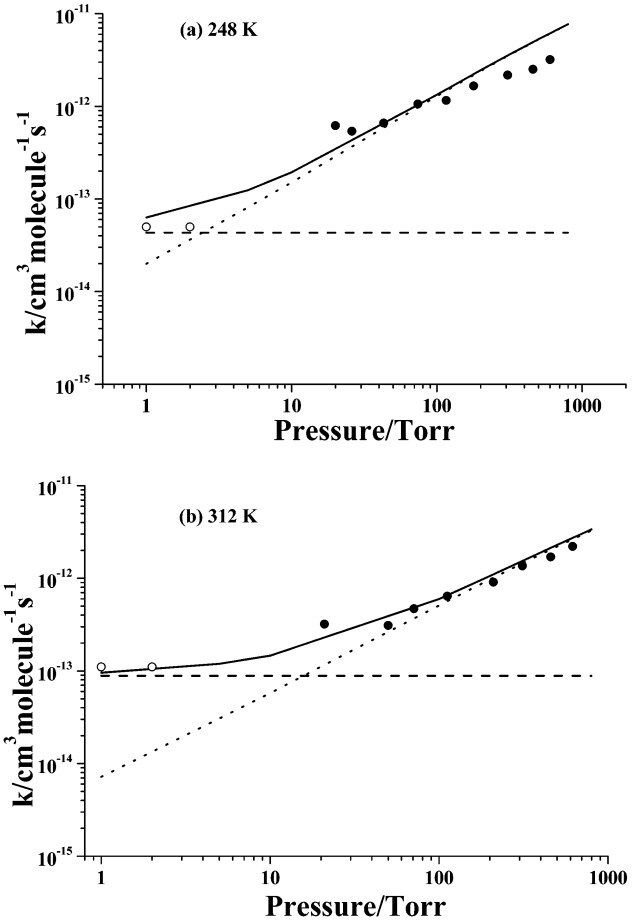

Figure 3. Comparison of the predicted and experimental pressure-dependent rate constants at 248 K (a) and 312 K (b) in Ar. Dotted, dashed, and solid lines are the predicted association, abstraction, and total rate constants, respectively. Symbols are experimental data taken from (●) ref 7 and (○) ref 8.

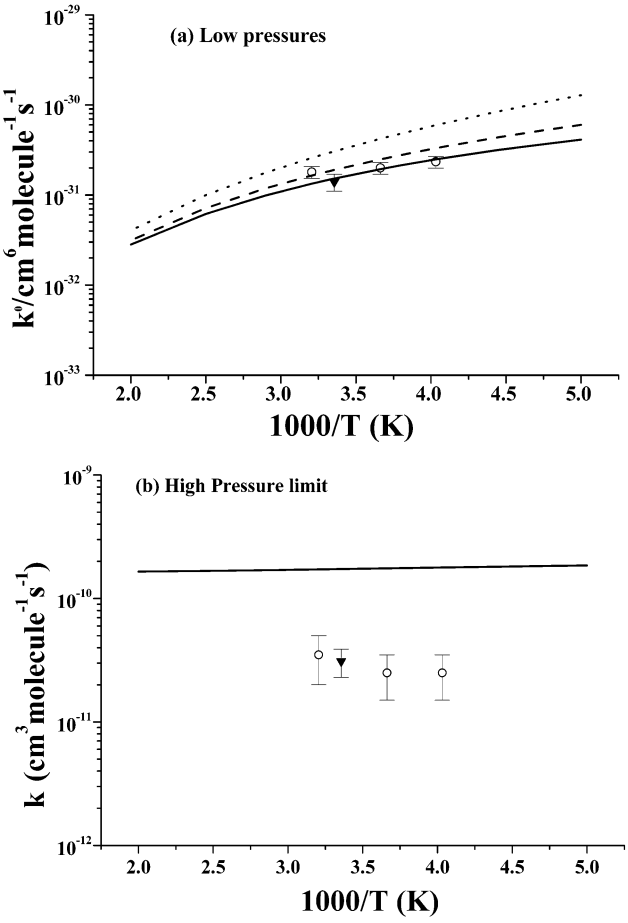

Figure 4. Comparison of the predicted and experimental available (a) low- and (b) high-pressure limit rate constants in Ar. Dotted, dashed, and solid lines are the predicted values at 10^{-4}, 100, and 760 Torr, respectively. Symbols are the experimental extrapolated data from (▼) ref 6 and (○) ref 7.

derived from deconvoluting the L-J potential of the He−ClO_3 system obtained by our ab initio calculation at the PW91PW91/6-311+G(3df) level using the approximations $\epsilon_{12} = (\epsilon_1\epsilon_2)^{1/2}$ and $\sigma_{12} = (\sigma_1+\sigma_2)/2$ for the collision pair. The ϵ_{12} and σ_{12} parameters for the He−ClO_3 collision pair were determined to be 53 K and 3.1 Å by fitting the L-J function,[31] $V = 4\epsilon[(\sigma/r)^{12} - (\sigma/r)^6]$. The L-J ($\epsilon_2$ and σ_2) parameters of He and Ar are taken from the literature.[31]

Thermal Decomposition of s-ClO_3. The unimolecular decomposition of s-ClO_3 has not been experimentally studied. The predicted high- and low-pressure limiting rate constants for the decomposition reaction $ClO_3 \rightarrow {}^3O + OClO$ can be expressed by

$$k_2^{\infty} = 1.5 \times 10^{20} T^{-1.1} \exp(-18360/T)\ s^{-1}$$

$$k_2^{0} = 3.76 \times 10^{25} T^{-3.28} \exp(-13890/T)\ cm^3\ mol^{-1}\ s^{-1}$$

in the temperature range 500−2500 K in Ar.

Bimolecular Association/Decomposition Reactions. The calculated pressure-dependent rate constants in Ar for $^3O + OClO \rightarrow ClO_3$ at 248 and 312 K are displayed in Figure 3a,b for comparison with experimental data.[7,8] $\langle\Delta E_{down}\rangle = 300\ cm^{-1}$ was used in the calculation. The experimental results show strong *P*-dependence with nonzero intercepts reflecting the convolution of the abstraction and association reactions.[6−8] These experimental data can be reasonably accounted by the sum of the predicted abstraction (k_3) and association (k_{-2}) values. Parts a and b of Figure 3 clearly show that at 248 and 312 K, the abstraction channel is dominant at the pressures below 3−10 Torr, depending on temperature. Our predicted total rate constants are in good agreement with the experimental values obtained by Stief and co-workers[8] at low pressures (1−5 Torr) and the values obtained by Colussi et al.[7] at medium pressures (20−600 Torr).

In Figure 4a, the predicted rate constants from 10^{-4} to 760 Torr are plotted to compare with available data. It shows that the extrapolated values[7] did not reach the real low-pressure limit, caused in part by the presence of the abstraction channel, which reduces the slope of the *k* vs *P* plot at low pressures. The predicted low-pressure limit rate constant for the O + OClO → s-ClO_3 association process can be expressed as $k_{-2}^0 = 7.0 \times 10^{-20} T^{-4.46} \exp(-217/T)$ cm^6 molucule^{-2} s^{-1} in the temperature range 200−500 K with Ar as the third body. Figure 4b shows that the predicted high-pressure limit rate constants are a factor of 7, 7, and 5 higher than the extrapolated values[7] at 248, 273, and 312 K, respectively, presumably due to the insufficient extrapolation of experimental data. The predicted high-pressure limit for O + OClO → s-ClO_3 can be expressed as $k_{-2}^{\infty} = 1.17 \times 10^{-10} T^{-0.039} \exp(51/T)$ cm^3 molucule^{-1} s^{-1} in the temperature range 200−500 K.

Figure 5 shows the comparison of predicted and experimental temperature-dependent rate constants for O + OClO mostly measured at He pressure near 1 Torr, with $\langle\Delta E_{down}\rangle = 150\ cm^{-1}$ for collisional stabilization. The results show that from 200 to 225 K, the rate constant decreases with temperature with the

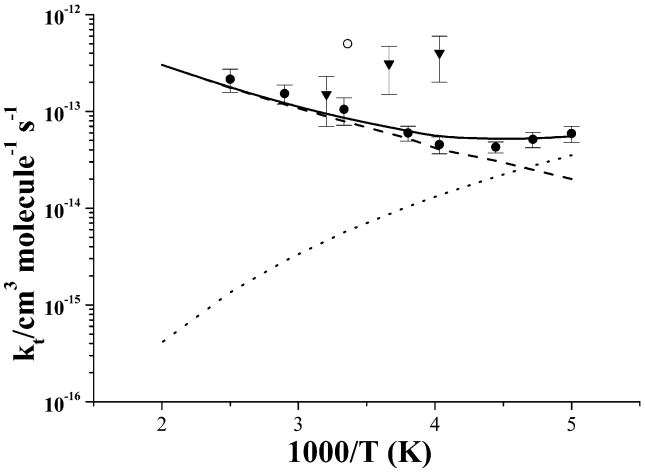

Figure 5. Comparison of the predicted and experimental temperature-dependent rateconstants in He at 1 Torr. Dotted, dashed, and solid lines are the predicted association, abstraction, and total rate constants, respectively. Symbols are experimental available data from (●) ref 8 (mostly obtained near 1 Torr He pressure), (▼) ref 7, and (○) ref 10.

association process being dominant. Over 225 K, the rate constant shows a positive temperature dependence, which is contributed by the abstraction channel, $^3O + OClO \rightarrow ClO + {}^3O_2$. Our predicted total rate constants are in good agreement with the experimental values of Stief and co-workers,[8] but inconsistent with the extrapolated values of Colussi et al.[7] from their high-pressure results (20−600 Torr in Ar) at 1 Torr. The association and abstraction rate constants in the temperature range 200−500 K can be expressed respectively as: $k_{-2} = 40.1T^{-6.16} \exp(-403/T)$ and $k_3 = 1.0 \times 10^{-16}T^{1.44} \exp(-469/T)$ cm^3 molecule^{-1} s^{-1}. The abstraction rate constants for 500−2500 K can be expressed as $k_3 = 8.69 \times 10^{-17}T^{1.45} \exp(-441/T)$ cm^3 molecule^{-1} s^{-1}.

IV. Conclusion

The unimolecular decomposition of the symmetric ClO_3 radical and the bimolecular abstraction and association processes of O + OClO have been studied by ab initio MO and statistical theory calculations. The ab initio results show that s-ClO_3 decomposes primarily by barrierless dissociation producing O + OClO, instead of the commonly assumed ClO + O_2 products, which require significantly higher barriers (5.6 and 16.9 kcal/mol above O + OClO). The O + OClO → ClO + $^3O_2$ abstraction reaction occurs with a 1.5 kcal/mol barrier. The calculated rate constants indicated that the association process has a strong positive-pressure and a small negative-temperature dependence. The V-shape Arrhenius plot observed by Stief and co-workers[8] at 1−5 Torr He, can be attributed to the combination of the association and abstraction processes. At $T < 225$ K, the association process dominates with a negative-temperature dependence, whereas at $T > 225$ K, the direct abstraction channel becomes dominant with a positive-temperature dependence. The predicted *P*,*T*-dependent bimolecular rate constants are in good agreement with available experimental values.

Acknowledgment. This work is sponsored by the Office of Naval Research under contract no. N00014-89-J 1949, Dr. J. Goldwasser program manager.

References and Notes

(1) Brill, T. B.; Budenz, B. T. In *Slod Propellant Chemistry, Combustion, and Motor Interior Ballistics*; Yang, V., Brill, T. B., Ren, W.-Z., Eds.; *Progress in Astronomy and Aeronautics, Vol. 185*; American Institute Aeronautics and Astrononomy, Inc.: VA, 20191, 2001; pp 3−32.
(2) Molina, M. J.; Colussi, A.; Molina, L. T.; Schindler R. N.; Tso, T−L. *Chem. Phys. Lett.* **1990**, *173*, 310.
(3) Zhu, R. S.; Lin, M. C. *Phys. Chem. Commun.* **2001**, *26*, 1.
(4) Wengax, X.; Baoxuan, L.; Kexiu, W. *Acta Astronautic.* **1987**, *15*, 83.
(5) Bemand, P. P.; Clyne, M. A. A.; Watson, R. T. *J. Chem. Soc., Faraday Trans.* **1973**, *69*, 1356.
(6) Colussi, A. *J. Phys. Chem.* **1990**, *94*, 8922.
(7) Colussi, A.; Sander, S. P.; Friedl, R. R. *J. Phys. Chem.* **1992**, *96*, 4442.
(8) Gleason, J. F.; Nesbitt, F. L.; Stief, L. J. *J. Phys. Chem.* **1994**, *98*, 126.
(9) Mauldin, R. L.; Burkholder, J. B., III; Ravishankara, A. R. *Int. J. Chem. Kinet.* **1997**, *29*, 139.
(10) Bemand, P. P.; Clyne, M. A. A.; Watson, R. T. *J. Chem. Soc., Faraday Trans.* **1973**, *1*, 1356.
(11) Mebel, A. M.; Morokuma, K.; Lin, M. C. *J. Chem. Phys.* **1995**, *103*, 7414.
(12) (a) Burke, K.; Perdew, J. P.; Wang, Y. In *Electronic Density Functional Theory: Recent Progress and New Direction*; Dobson, J. F., Vignale, G., Das, M. P., Eds.; Plenum: New York, 1998. (b) Perdew, J. P. In *Electronic Structure of Solids' 91*; Ziesche, P., Eschrig, H., Eds.; Akademie Verlag: Berlin, 1991; p 11. (c) Perdew, J. P.; Chevary, J. A.; Vosko, S. H.; Jasckson, K. A.; Pederson, M. R.; Singh, D. J.; Fiolhais, C. *Phys. Rev.* **1992**, *B46*, 6671. (d) Perdew, J. P.; Burke, K.; Wang, Y. *Phys. Rev.* **1996**, *B54*, 16533.
(13) Gonzalez, C.; Schlegel, H. B. *J. Phys. Chem.* **1989**, *90*, 2154.
(14) Frisch, M. J.; Trucks, G. W.; Head-Gorden, M.; Gill, P. M. W.; Wong, M. W.; Foresman, J. B.; Johnson, B. G.; Schlegel, H. B.; Robb, M. A.; Replogle, E. S.; Gomperts, R.; Andres, J. L.; Rahavachari, K.; Binkley, J. S.; Gonzalez, C.; Martin, R. L.; Fox, D. J.; Defrees, D. J.; Baker, J.; Stewart, J. J. P.; Pople, J. A. *Gaussian 98*; Gaussian, Inc.: Pittsburgh, PA, 1998.
(15) Klippenstein, S. J.; Wagner, A. F.; Dunbar, R. C.; Wardlaw, D. M.; Robertson, S. H. VARIFLEX: VERSION 1.00, 1999.
(16) Gilbert, R. G.; Smith, S. C. *Theory of Unimolecular and Recombination Reactions*; Blackwell Scientific: Carlton, Australia, 1990.
(17) Holbrook, K. A.; Pilling, K. J.; Robertson, S. H. *Unimolecular Reactions*; Wiley: Chichester, U.K., 1996.
(18) Rathmann, T.; Schindler, R. N. *Ber. Bunsen-Ges. Phys. Chem.* **1992**, *96*, 421.
(19) Rauk, A.; Tschuikow-Roux, E.; Chen, Y. H.; McGrath, M. P.; Radom, L. *J. Phys. Chem.* **1993**, *97*, 7947.
(20) Workman, M. A.; Francisco J. S. *Chem. Phys. Lett.* **1997**, *279*, 158.
(21) Janoschek, R. *J. Mol. Struct. (THEOCHEM)* **1998**, *423*, 219.
(22) Beltrán, A.; Andrés, J.; Noury, S.; Silvi, B. *J. Phys. Chem. A* **1999**, *103*, 3078.
(23) Alcami, M.; Mó, O.; Yáñez, M.; Cooper, I. L. *J. Chem. Phys.* **2000**, *112*, 6131.
(24) Grothe, H.; Willner, H. *Angew. Chem., Int. Ed. Engl.* **1994**, *33*, 1482.
(25) Rathmann, T.; Schindler, R. N. *Chem. Phys. Lett.* **1992**, *190*, 539.
(26) Chase, M. W., Jr. *NIST-JANAF Thermochemical Tables*, 4th ed.; Woodbury, NY, 1998.
(27) Wardlaw, D. M.; Marcus, R. A. *Chem. Phys. Lett.* **1984**, *110*, 230; *J. Chem. Phys.* **1985**, *83*, 3462.
(28) Klippenstein, S. J.; Marcus, R. A. *J. Chem. Phys.* **1987**, *87*, 3410.
(29) Chen, W.; Schlegel, H. B. *J. Chem. Phys.* **1994**, *101*, 5958.
(30) Krylov, A. I. *Chem. Phys. Lett.* **2001**, *338*, 375.
(31) Hirschfelder, J. O.; Curtiss, C. F.; Bird, R. B. *Molecular theory of gases and liquids*, 2nd ed.; John Wiley and Sons Inc.: New York, 1964.